Self-Centering Precast Concrete Dual-Shell Steel Columns

Gabriele Guerrini & José I. Restrepo
University of California - San Diego, La Jolla, California, USA

Milena Massari & Athanassios Vervelidis
Alma Mater Studiorum - University of Bologna, Italy

SUMMARY
The testing, modeling, and design of an innovative bridge column technology for application in seismic regions is presented in this paper. This structural solution combines a precast concrete hollow-core column with self-centering behavior and energy dissipation. The column consists of two steel shells running for its full-height, with concrete sandwiched in between. The shells act as permanent formwork, the outer one substituting longitudinal and transverse reinforcement, the inner one preventing concrete implosion. Large inelastic rotations can be attained at the end joints with minimal structural damage, since gaps are allowed to open in tension at these interfaces and to close upon load reversal. Self-centering behavior is ensured by post-tensioned longitudinal bars, which are designed to respond elastically. Energy dissipation is provided by internal or external steel devices which are allowed to yield axially. Experimental findings from quasi-static tests are shown, and numerical simulations of the tests as well as design considerations are discussed.

Keywords: Column, Concrete, Energy Dissipation, Precast Concrete, Self-centering.

1. INTRODUCTION

Current seismic design philosophies for ductile reinforced concrete bridges (Caltrans, 2010) allow them to respond beyond the elastic limit, with the inelastic behavior localized within plastic hinge regions at the bottom and/or top of the pier elements. The system is therefore built with regions that will be sacrificed during moderate and strong earthquakes and may require from minor to expensive repair work. In addition, the occurrence of severe damage or partial collapse of a bridge system can lead to critical consequences associated to the interruption of a fundamental road path, such as obstruction of rescue and recovery operations and economical losses related to business interruption, displacement of people, and goods (Palermo et al., 2008). While the notion of structural damage is accepted in design, resilient communities expect bridges to survive a moderately strong earthquake with little or no disturbance to traffic: this implies that partial or total bridge closures are tolerated with uneasiness, particularly in heavily congested urban areas. As a consequence, research efforts have been prompted into advanced technologies that reduce residual damage to the main structural elements, and encompass self-centering properties which allow the structural system to return to its original position after an earthquake. Moreover, these innovative solutions need to be economically viable when compared to existing technologies (Guerrini et al., 2011).

The typical behavior of three alternative column solutions is schematized in Figure 1. A conventional monolithic structure (Fig. 1(a)) offers large energy dissipation, represented by “fat” hysteretic loops, at the expenses of structural integrity and significant residual deformations. A purely rocking column (Fig. 1(b)) is characterized by non-linear elastic behavior, due to opening of a gap at the base and eventually at the top, with self-centering properties ensured by gravity and post-tensioning forces; however, very little dissipation is achieved herein. A hybrid-rocking system (Fig. (1c)) provides a trade-off between these two extremes: balancing self-centering forces with additional energy dissipation leads to a flag-shaped response, with small residual displacements but relatively fat loops.

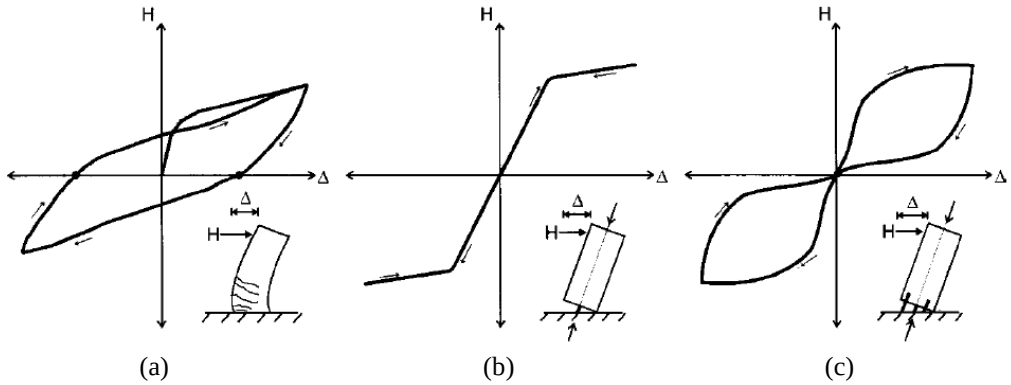

Figure 1. Schematic comparison between hysteretic responses: (a) conventional monolithic system; (b) rocking system; (c) hybrid rocking system (Holden et al., 2003).

In response to the mentioned needs, researchers at the University of California, San Diego (UCSD) are developing a *Self-Centering Precast Concrete Dual-shell Steel Column* solution for bridge piers, which can be ascribed in the hybrid-rocking category (Tobolski, 2010; Guerrini et al., 2012). Use of precast members, replacement of traditional time-consuming reinforcing cages with steel pipes, and adoption of hollow cross-sections resulting in weight reduction, are aimed to improve constructability and to reduce on-site burdens. In parallel, the combination of unbonded post-tensioned joint connections with specific energy dissipating devices ensure seismic resilience, in the form of self-centering capability, facilitation of structural fuse repair, and minimization of damage to the main structural elements. As a consequence, traffic impacts, environmental disruptions, and life-cycle costs can be reduced, responding to an initiative of the US Federal Highway Administration (FHWA) denominated *Accelerated Bridge Construction* (ABC).

2. SYSTEM DESCRIPTION

The system developed at UCSD combines a precast concrete hollow-core column with on-site post-tensioning and supplemental energy dissipation. The column consists of two concentric cylindrical steel shells (*dual-shell* technology) that run for the full-height of the column, with concrete sandwiched in between, as shown in Figure 2(a). The outer shell acts as permanent formwork, and provides longitudinal and transverse reinforcement. The inner shell also behaves as permanent formwork, and prevents concrete implosion under large compressive strains. Constructability is enhanced by the use of a precast element of reduced weight (hollow-core section) without a reinforcing cage (Tobolski, 2010; Guerrini et al., 2011).

Large non-linear rotations can be attained with minimal structural damage. These rotations are accommodated within the connections themselves, through the formation of gaps at the column-footing and column-bent cap interfaces (Fig. 2(b)): gaps are allowed to open in tension under severe lateral displacement demand, and to close subsequently upon load reversal. Self-centering/rocking properties are provided by gravity forces and one or more unbonded post-tensioning (PT) bars, designed to respond elastically. A special connection between column, bent cap, foundation, and PT bars allows for eventual bar replacement, should corrosion or other damage to the bar be a concern.

Energy dissipation takes place through extensive yielding of internal dowel bars (Restrepo et al., 2007; Tobolski, 2010), as shown in Figure 2(b), or external devices (Marriott et al., 2009; Toranzo et al., 2009), preventing the main structural members from suffering significant damage. Under a strong-intensity shake only these devices are expected to undergo multiple cycles within the inelastic range of response, with possible need of replacement, but the structure is expected to remain functional overall.

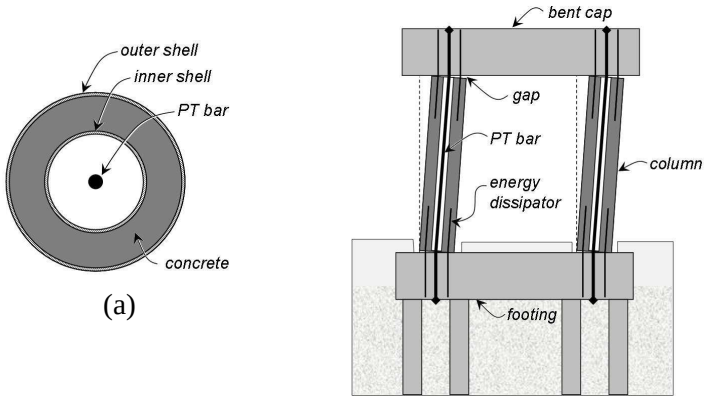

Figure 2. Sketches of the proposed system: (a) column cross-section; (b) bent components and kinematics.

In order to obtain a flag-shaped hysteretic response, the self-centering forces (gravity and post-tensioning) must be large enough to overcome the overstrength capacity of the energy dissipators, thus forcing them in compression and closing the gap at each load reversal (Restrepo et al., 2007). Care must be paid to prevent post-tensioning losses due to yielding of the PT bars or crushing of the mortar that seals the joints. The first issue is addressed by placing rubber or urethane pads at the bar anchorage, thus adding a source of elastic deformability in series with the bars. The use of a high-performance, fiber-reinforced mortar can instead retard crushing.

3. EXPERIMENTAL PROGRAM

3.1 Test specimens

Two *dual-shell* column specimens were tested at the UCSD Powell Structural Engineering Laboratories: unit 1A incorporated external buckling-restrained energy dissipators, while unit 1B had internal dowel bars. They were loaded in a cantilever configuration, with fixed base and lateral forces applied at the top, as shown in Figure 3(a). Given the precast nature of footing, column, and load stub, it was possible to assemble them as unit 1A, take them apart after the first test, and reconnect them as unit 1B. In fact, since only the bottom region of the column was subjected to large strains during the first test, the same column could be flipped upside-down and reused in the second specimen, taking advantage of both ends (Massari, 2012; Vervelidis, 2012; Guerrini et al., 2012).

The column had an overall diameter of 0.51 m (20 in.) and a height of 0.84 m (33 in.); the total cantilever span above the footing to the point of lateral load application was 1.13 m (44.5 in.). A low aspect ratio of 2.2 was chosen to induce a large ultimate base shear, thus leading to a more critical condition for sliding. Moreover, a short element can accommodate short post-tensioning bars, which are more susceptible to yielding due to their lower axial deformability.

The external diameter of the column outer shell was 0.51 m (20 in.) and its thickness 6.4 mm (0.25 in.), while the inner shell had an external diameter of 0.36 m (14 in.) and a thickness of 3.2 mm (0.125 in.), as shown in Figure 3(b). Both shells were obtained folding and welding plates made of A572 Grade 50 steel. High-strength, normal-weight concrete was used to cast column, footing, and load stub. The specified concrete compressive strength at 56 days was 62 MPa (9.0 ksi), the ones measured at 28 days, 49 days (day of testing of unit 1A) and 96 days (day of testing of unit 1B) were 66 MPa (9.5 ksi), 70 MPa (10.2 ksi), and 72 MPa (10.4 ksi), respectively. Six radially distributed 12.7-mm (0.5-in.) thick steel brackets were welded to the outer shell (Fig. 3(b), above) for the installation of the external dissipators of unit 1A. Six 50.8-mm (2-in.) diameter, 0.46-m (18-in) long, corrugated metal ducts were left in the concrete for the installation of the internal dowels of unit 1B (Fig. 3(b), below); three circumferential 9.5-mm (3/8-in.) weld beads on the internal surface of the outer shell provided tensile stress transfer between the dowels and the shell.

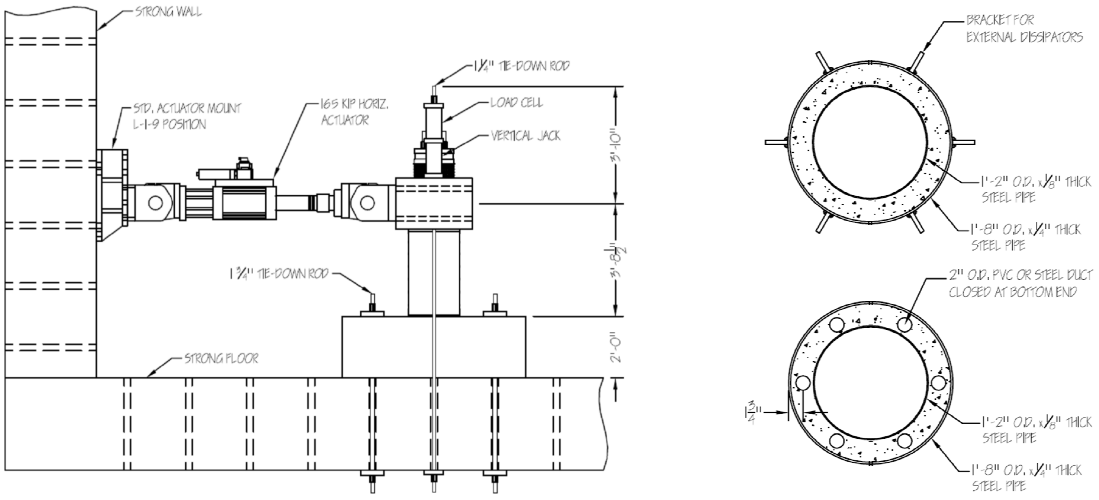

(a) (b)

Figure 3. Specimen drawings: (a) test setup; (b) column base cross-sections for unit 1A (above) and 1B (below).

A 12.7-mm (0.5-in.) thick mortar layer was created between column and footing, to compensate for lack of precision in the construction and positioning of the precast members. Upon rocking, large compressive strains arise on the mortar, making a high-perofrmance material necessary to prevent crushing and subsequent PT losses. BASF Embeco 885 grout with plastic consistency was used in unit 1A, with a measured compressive strength of 46.4 MPa (6.7 ksi) and 49.2 MPa (7.1 ksi) at 29 and 49 days (day of testing of unit 1A), respectively. For the bottom joint of unit 1B the same mix was used, with the addition of polypropylene fibers in the proportion of 0.035% by weight to increase the material ductility; strengths of 53.4 MPa (7.8 ksi) and 52.9 MPa (7.7 ksi) were obtained at 28 and 35 days (day of testing unit 1B). The upper joint between column and load stub, not critical because of the low bending moment at this location, was realized with hydrostone in both specimens. All interface surfaces were roughened to improve shear friction. Bond breaker was applied to the bottom surface of the column, to allow separation from the mortar bed and opening of the gap.

Six external energy dissipating devices were incorporated in test unit 1A, radially distributed around the perimeter (Fig. 4). They were obtained from steel bars with a reduced diameter over a specific length, where the dissipation was provided by hysteresis of the material. Each 343-mm (13.5-in.) long steel bar had a virgin diameter of 25.4 mm (1 in.), which was reduced to 14.3 mm (9/16 in.) in the dog-bone milled part for a length of 165 mm (6.5 in.). Hot-rolled A576 Grade 1018 steel was used for the external dissipators, with measured yield strength of 331 MPa (48 ksi), ultimate strength of 490 MPa (71 ksi), and ultimate strain of 33.9%. In order to prevent buckling, the milled part was encased in a steel pipe and grouted; grease was used to reduce friction between bar and grout. The devices were welded to anchors within the footing and to the column outer shell brackets.

Unit 1B was equipped with six internal dowels at the column-footing joint, acting as internal energy dissipators (Fig. 5). 316LN Grade 75 stainless steel #4 rebars were used for this purpose, debonded by duct-tape wrapping for 178 mm (7 in.) across the interface to confine yielding within this segment. Material testing provided a yield stress of 745 MPa (108 ksi), ultimate strength of 889 MPa (129 ksi), and ultimate strain of 25.7%. The dowels were first grouted within corrugated steel ducts predisposed in the footing, then, after column placement on the footing, they were grouted within the column ducts. The footing grout had a compressive strength of 52.7 MPa (7.6 ksi) on the day of testing, while the column grout had 59.2 MPa (8.6 ksi); in both cases, Embeco 885 with fluid consistency was used.

Post-tensioning was provided by four 34.9-mm (1-3/8 in.) diameter, A722 Grade 150 DSI Threadbars. The total effective post-tensioning force was 801 kN (180 kips) in unit 1A and 890 kN (200 kips) in unit 1B, after losses. The bars were running within the column hollow core, sleeved in ducts filled with fluid BASF Embeco 885 grout to simulate corrosion protection. The PT bars were screwed into anchorage devices prearranged in the footing (Fig. 6(a)), to allow for subsequent replacement.

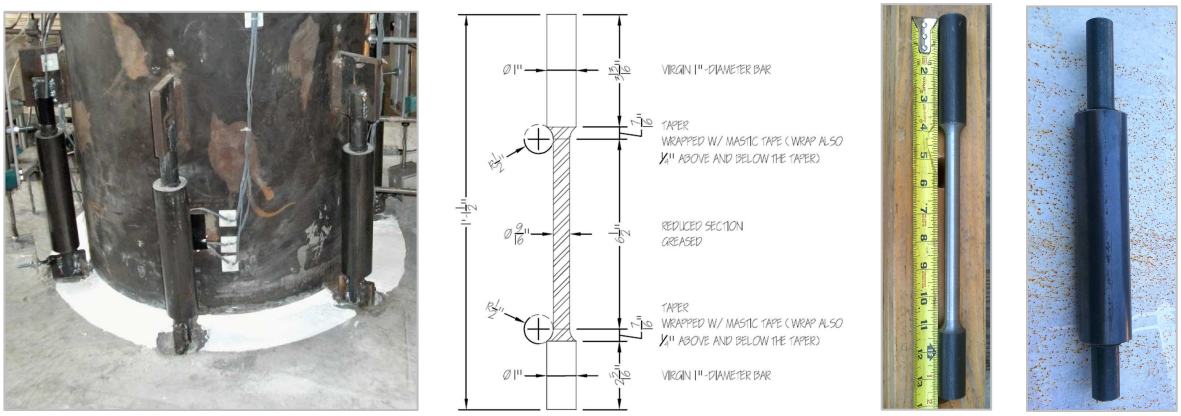

(a) (b) (c) (d)

Figure 4. External energy dissipators: (a) location around column perimeter; (b) construction details; (c) dog-bone milled steel bar; (d) assembled buckling-restrained device.

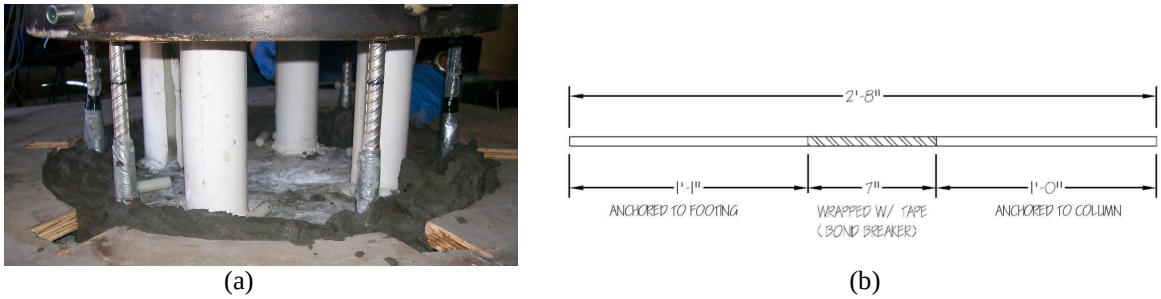

(a) (b)

Figure 5. Internal energy dissipators: (a) dowels during column placement; (b) construction details.

The PT bars were screwed into anchorage devices prearranged in the footing (Fig. 6(a)), to allow for subsequent replacement. In order to preserve the self-centering capacity of the system it is important that, upon gap opening, the tensile strain increment on the PT bars does not lead them to yielding. For this reason, additional deformability was provided in series with the post-tensioning bars by placing rubber or polyurethane bearings between the top anchorage plates and the load stub. With this configuration the tensile deformation demand on the bars was partially transformed into compressive deformation of the rubber pads.

A bearing made of five square rubber pads alternated with six square steel plates, with central holes to accommodate the bars, was provided to each PT bar in test unit 1A (Fig. 6(b)); each bearing had a stiffness equal to 1.46×105 kN/m (836 kip/in). SA-47 rubber pads, produced by Fabreeka International, were used. A bearing made of four Fyfe discs alternated with five circular steel plates, with central holes to accommodate the bars, was provided to each PT bar in test unit 1B (Fig. 6(c)); each bearing had a stiffness equal to 4.38×104 kN/m (250 kip/in). Fyfe discs were made of 90-durometer-A adiprene, a special polyurethane material developed by Edward Fyfe.

(a) (b) (c)

Figure 6. PT bar anchorages: (a) within the footing, with holes for external dissipator anchorages also visible; (b) unit 1A, rubber bearings above load stub; (b) unit 1B, Fyfe-disc bearings above load stub.

3.2 Testing protocol and results

A vertical load, simulating gravity forces, was applied to the specimen by two vertical jacks, positioned above the load stub and connected to the strong floor by one 31.8-mm (1-1/4 in) diameter tie-down rod each (Fig. 3(a)). Actual loads of 293 kN (63 kips) and 268 kN (60 kips) were applied to unit 1A and unit 1B, respectively. Keeping the vertical force constant, the test unit was subjected to quasi-static reversed cyclic loading by a horizontal actuator in the north-south direction. After three force-controlled cycles to ±111 kN (25 kips) and three to ±231 kN (52 kips) base shear, the test proceeded in displacement control. Three cycles to ±0.5% drift ratio and 3 to ±0.5% were completed. Subsequent cycles composed of two large amplitude cycles, followed by a lower one at a level corresponding to the previous large drift level: drift ratios of ±1%, ±1.5%, ±2%, ±3%, ±5%, ±7.5%, and ±10% were targeted. Figure 7 shows the hysteretic lateral force-displacement response of the two units. Lateral displacements are normalized by the cantilever span and thus expressed as drift ratios, while lateral forces are normalized by the applied gravity load (equivalent to the weight) and thus transformed into base shear coefficients.

3.2.1 Unit 1A

Testing of unit 1A resulted in cracks forming at the column-mortar bed interface during the cycles to ±231 kN (52 kips) base shear; as a consequence a first loss of stiffness was observed on the diagram of Figure 7(a). The mortar bed started flaking during ±1.5% drift-ratio cycles, and showed extensive flaking and permanent compressive deformation on the north and south sides (extreme fibers) during ±3% drift-ratio cycles (Fig. 8(a)), causing a sudden loss of stiffness. The mortar bed started crushing extensively during ±5% drift-ratio cycles, with significant loss of stiffness and self-centering ability.

External dissipators started bending between the buckling-restrained central portion and the end connections during ±3% drift-ratio cycles (Fig. 8(b)), due to the rotation imposed by the rocking kinematic. The north-west dissipator fractured during the first negative cycle to -7.5% drift ratio, nearly at peak displacement. Two other dissipators fractured on the south side during subsequent cycles. Each fracture corresponded to a jump on the graph of Figure 7(a). Due to failure of three out of six dissipators, the test was interrupted after the first cycle to ±10% drift ratio. The conditions of the specimen at the end of the test are shown in Figure 8(c): extensive mortar crushing is visible, as well as distortion and fracture of energy dissipators.

3.2.2 Unit 1B

Similarly to the previous case, testing of unit 1B resulted in cracks forming at the column-mortar bed interface during the cycles to ±231 kN (52 kips) base shear; as a consequence a first loss of stiffness was observed on the diagram of Figure 7(b). The mortar bed started flaking during ±2% drift-ratio cycles, and showed extensive flaking and permanent compressive deformation on the north and south sides (extreme fibers) during ±3% drift-ratio cycles, causing a sudden loss of stiffness. Mortar bed crushing progressed during ±5% drift-ratio cycles, but not abruptly; it became extensive under ±7.5% drift-ratio cycles, when the stiffness was evidently reduced as well as the self-centering capacity.

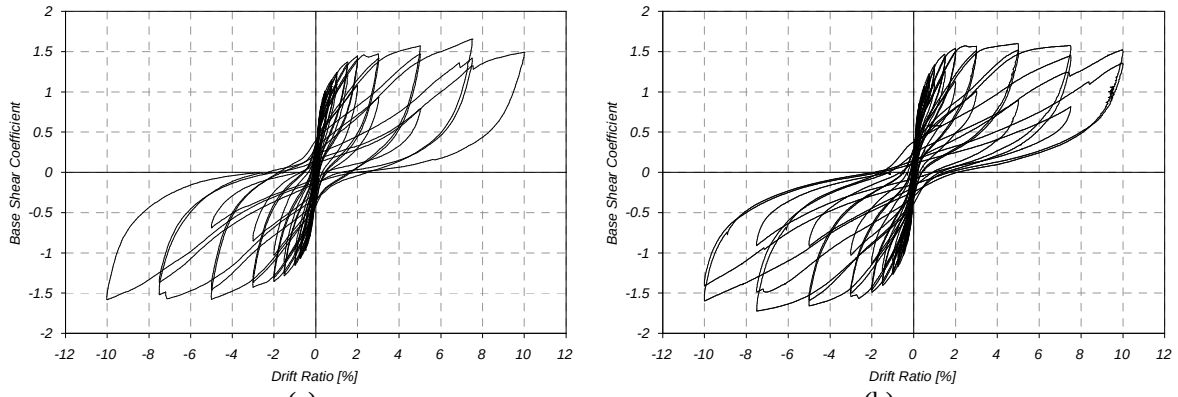

(a) (b)

Figure 7. Hysteretic lateral force-displacement response: (a) unit 1A; (b) unit 1B.

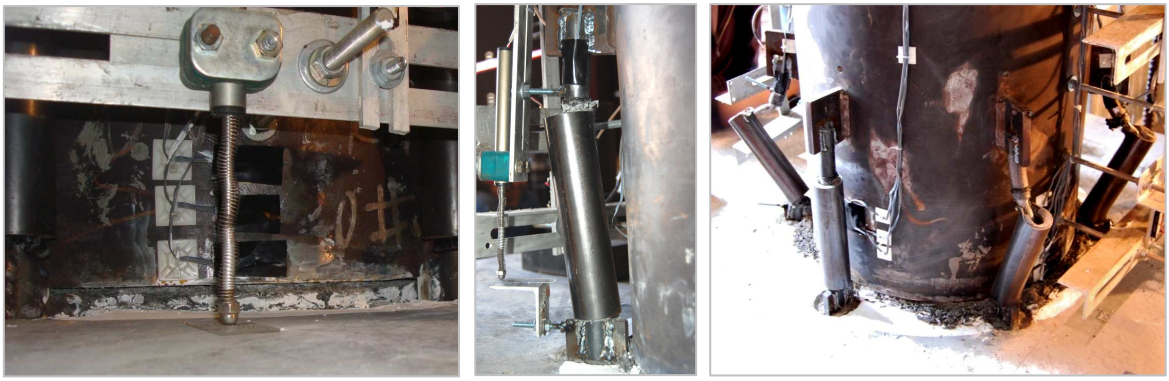

(a) (b) (c)

Figure 8. Testing of unit 1A: (a) mortar bed flaking during ± 3% drift-ratio cycles; (b) dissipator distortion during ± 5% drift-ratio cycles; (c) specimen at the end of the test.

(a) (b)

Figure 9. Unit 1B after testing: (a) crushed mortar bed; (b) permanent deformations of concrete and steel shells.

A first dissipator fractured on the north side during the second negative cycle to -7.5% drift ratio, nearly at peak displacement. A second dissipator fractured on the north side and two on the south side during subsequent cycles. Each fracture corresponded to a jump on the graph of Figure 7(b). The conditions of the specimen at the end of the test are shown in Figure 9. Extensive mortar crushing is visible in Figure 9(a). Permanent compressive deformation of the column concrete between the shells, and permanent deformation of the shells themselves due to concrete lateral expansion, is shown in Figure 9(b); the same residual damage was also observed at the other end after unit 1A test.

4. NUMERICAL MODELING

A 3D numerical model of the tests was built and validated with the experimental results. For this purpose the software OpenSees, developed by the Pacific Earthquake Engineering Research Center (PEER), was used. Details can be found in Vervelidis, 2012, and Guerrini et al., 2012.

The column was modeled with two elastic frame elements in series, connected to the mortar joint at the base and to the load stub at the top; the intermediate node was needed to link the energy dissipator elements. Multiple non-linear truss elements represented the mortar at the interface between column and footing; the length of each element accounted for spreading of inelastic behavior within the column, modeled as elastic; *Concrete01* non-linear material model was used. The post-tensioning bars were modeled as non-linear truss elements, with an initial stress equal to the effective prestress, and an equivalent stiffness accounting for the rubber bearings in series with the bars; they were fixed at the base and connected to the top node of the column by rigid elements. External energy dissipating devices for test unit 1A were represented by non-linear frame elements, as well as internal dowel bars for unit 1B; in both cases, the dissipators' lower ends were fixed to the footing, and their upper ends were connected to the column intermediate node by rigid links. *Steel02* non-linear material model was assigned to PT bars and dissipators. A node was introduced just above the column, at a distance equal to half the load stub height, for the application of the vertical load and lateral displacement history;

since the deformations of the loading stub are expected to be negligible, the node created in that position was linked to the top of the column with a rigid element.

The analysis was performed in two stages: first, the vertical load was applied and held constant; then the cyclic quasi-static lateral displacement history was assigned to the load stub centroid. The Newton-Raphson algorithm was chosen to solve the nonlinear residual equation. The analysis was performed under the hypothesis of small displacements, or *linear geometric transformation* in OpenSees language: in fact the vertical load was applied using tie-down rods, which were leaning together with the column under lateral displacement; as a consequence, the applied force was always directed along the column axis with no interaction between axial load and lateral displacement. Special care was given to reproduce the system behavior for drift ratios up to 5%, since larger displacements would be too demanding for a bridge superstructure. Moreover, modeling the material behavior near collapse requires the implementation of complicated routines and the knowledge of parameters that were not available from experimental tests.

The comparison between experimental and numerical results up to 5% drift ratio shows an accurate representation of the strength, stiffness, and self-centering capacity of the system. In the case of unit 1A (Fig. 10(a)) the numerical model slightly overestimates the stiffness of the system, predicting higher lateral forces in particular after 2% drift-ratio cycles; in the case of unit 1B (Fig. 10(b)), instead, the model underestimates the stiffness for drifty ratios between 1% and 3%. The hysteretic axial strain-stress response of the north-west external dissipator of unit 1A is also satisfactory captured by the model (Fig. 10(c)): the different behavior in tension and compression, observed from experimental data and due to the additional compressive strength provided by the grout in the buckling-restrained segment, is well reproduced by the model; an overestimation of the dissipator strength, both in tension and compression, is visible for low drift-ratio cycles. Figure 10(d) show a comparison between numerical and experimental strain histories of the south-west PT bars of unit 1B up to 5% drift ratio: good agreement is observed, in particular for values of drift ratio between 1% and 3%; a slight overestimation of the tensile strains is evident at higher drift ratios. The progressive loss of prestress due to gradual failure of the mortar at the rocking interface is well captured by the model, resulting in a good prediction of the overall behavior of the system.

5. DESIGN CONSIDERAITONS

Hybrid systems require a good balance between self-centering (gravity and post-tensioning) and dissipating forces. In order to ensure self-centering behavior, the first ones need to be large enough to overcome the overstrength capacity of the energy dissipators; for this purpose, the following upper bound for the *self-centering index* Λ_C is suggested:

$$\Lambda_C = F_{ED,u} \Big/ \left(F_{PT,e} + P_u \right) \leq 0.70 \tag{1}$$

where $F_{ED,u}$ is the sum of all energy dissipators ultimate (peak) strength, $F_{PT,e}$ is the effective post-tensioning force after losses, and P_u is the design axial load. However, in order to provide a minimum dissipative force, a lower limit for the energy dissipation index Λ_D is also recommended (Restrepo et al., 2007):

$$\Lambda_D = F_{ED,u} \Big/ \left(F_{ED,u} + F_{PT,y} + P_u \right) \geq 0.10 \tag{2}$$

where $F_{PT,y}$ is the sum of the yield forces of all post-tensioning bars.

Another condition to be checked is that post-tensioning bars are not yielding under gap opening. For any joint rotation θ_j, the force $F_{PT}^{(b)}$ on bar *b*, located at a depth $d_{PT}^{(b)}$ from the extreme compressive fiber, is then limited by:

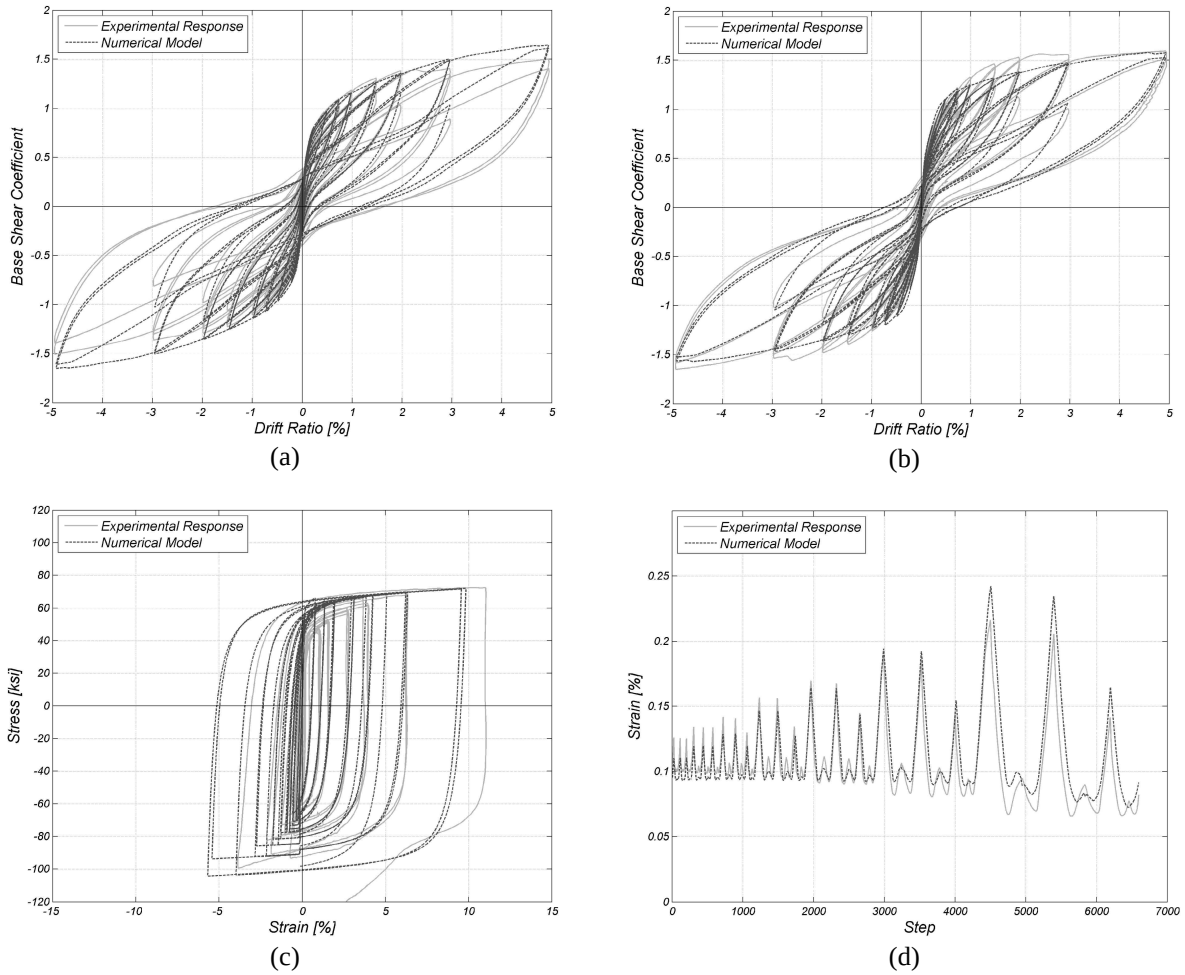

Figure 10. Comparison between numerical and experimental responses: (a) lateral force-displacement relationship for unit 1A; (b) lateral force-displacement relationship for unit 1B; (c) axial hysteretic behavior of north-west external dissipator in unit 1A; (d) axial strain history of south-west PT bar in unit 1B.

$$F_{PT}^{(b)} = F_{PT,e}^{(b)} + n_j \theta_j \left(d_{PT}^{(b)} - c \right) \frac{1}{\dfrac{L_{UPT}}{E_{PT} A_{PT}^{(b)}} + \dfrac{1}{K_{RB}}} \le F_{PT,y}^{(b)} \tag{3}$$

where $F_{PT,e}^{(b)}$ is the effective prestress on bar *b*, $F_{PT,y}^{(b)}$ its yield strngth , L_{UPT} its unbonded length, E_{PT} its elastic modulus, and $A_{PT}^{(b)}$ its area; n_j is the number of column ends subjected to joint rotation (1 or 2); *c* is the neutral-axis depth corresponding to θ_j ; and K_{RB} is the stiffness of the rubber or urethane bearing in series with the bar. The effective prestress should be limited to 25% of the yield strength, and the bearing stiffness can be adjusted to avoid premature bar yielding.

The base shear, V_B, should not exceed the shear-friction capacity at the interfaces at any drift ratio:

$$V_B \le \mu_f C_C \tag{4}$$

where μ_f is the shear-friction coefficient and C_C is the compressive resultant on the concrete. Moreover, to limit strain demands on concrete and mortar, the neutral axis depth, *c*, should not exceed 20% of the outermost column diameter, D_{out} , at the target design drift ratio:

$$c / D_{out} \le 0.20 \tag{5}$$

6. CONCLUSIONS

The use of internal dissipators in the form of longitudinal dowel bars (unit 1B), crossing the column-footing interface, offers the advantage of avoiding aesthetic interference. However, for inspection and replacement of damaged dissipators would require cutting and repairing the outer steel shell: for this reason, accessible external devices (unit 1A) could be advantageous. Improvements to the connections of external buckling-restrained devices are required in order to avoid bending of the bar ends. Dissipating and self-centering forces need to be well balanced using equations (1) and (2).

The adoption of post-tensioning bars instead of strands allows for re-tensioning or de-tensioning and replacement, in case of damage. Bars can be unscrewed from the foundation anchorage and substituted together with the grouted ducts which protect them from corrosion. The introduction of bearing pads at the top anchorage is effective in preventing PT bars from yielding.

The use of a high performance material retards mortar-bed crushing and subsequent PT loss, especially if polypropylene fibers are added to the mix. The neutral axis depth should be controlled, to limit strain demands on mortar and concrete. Shear sliding at the joint does not represent an issue even for short aspect-ratio members.

Comparison between experimental and numerical (OpenSees) responses shows satisfactory accuracy in terms of overall system behavior and single components response. The self-centering behavior was accurately represented up to 5% drift ratios.

AKCNOWLEDGEMENT

Funding for this project, provided by the Pacific earthquake Engineering Research Center (PEER) and by the California Department of Transportation (Caltrans), is gratefully acknowledged. The assistance of the technical staff of the Charles Lee Powell Structural Engineering Laboratories at the University of California, San Diego, and the participation of the students Giovanni De Francesco and Maura Torres, are duly acknowledged. The authors also thank Salit Specialty Rebars and Hill Brothers Chemical Co. for their support.

REFERENCES

Caltrans (2010). Seismic Design Criteria. California Dept. of Transportation, Sacramento, California, USA.

Guerrini, G., and Restrepo, J.I., (2011). Advanced Precast Concrete Dual-Shell Steel Columns. *8th International Conference on Urban Earthquake Engineering, Tokyo, Japan*. **Vol I:** 1125-1129.

Guerrini, G., Massari, M., Vervelidis, A., De Francesco, G., Torres, M., and Restrepo, J.I. (2012 in preparation). Advanced Self-Centering Precast Concrete Dual-Shell Steel Columns. *Research Report*, Pacific Earthquake Engineering Research Center, Berkeley, California, USA.

Holden, T., Restrepo, J.I., and Mander, J.B (2003). Seismic Performance of Precast Reinforced and Prestressed Concrete Walls. *ASCE Journal of Structural Engineering*. **129:3**, 286-296.

Marriott, D., Pampanin, S., and Palermo, A. (2009). Quasi-Static and Pseudo-Dynamic Testing of Unbonded Post-Tensioned Rocking Bridge Piers with External Replaceable Dissipaters. *Earthquake Engineering and Structural Dynamics*. **38:3**, 331-354.

Massari, M. (2012). Hybrid Precast Concrete Dual-Shell Steel Bridge Columns Under Lateral Loading. *Tesi di Laurea Specialistica*, Dept. of Civil, Environmental and Material Engineering, University of Bologna, Italy.

Palermo, A. and Pampanin, S. (2008). Enhanced Seismic Performance of Hybrid Bridge Systems: Comparison with Traditional Monolithic Solutions. *Journal of Earthquake Engineering*. **12:8**, 1267-1295.

Restrepo, J.I. and Rahman, A. (2007). Seismic Performance of Self-Centering Structural Walls Incorporating Energy Dissipators. *ASCE Journal of Structural Engineering*. **133:11**, 1560-1570.

Tobolski, M.J. (2010). Improving the Design and Performance of Concrete Bridges in Seismic Regions. *Ph.D. Thesis*, Dept. of Structural Engineering, University of California - San Diego, La Jolla, California, USA.

Toranzo, L.A., Restrepo, J.I., Mander, J.B., and Carr, A.J. (2009). Shake-Table Tests of Confined-Masonry Rocking Walls with Supplementary Hysteretic Damping. *Journal of Earthquake Engineering*. **13:6**, 882-898.

Vervelidis, A. (2011). Seismic Response of Self-Centering Precast Concrete Dual-Shell Steel Columns. *Tesi di Laurea Specialistica*, Dept. of Civil, Environmental and Material Engineering, University of Bologna, Italy.